Thermohaline mixing and extinction in stars

Report submitted for the application for transfer from M.Phil. to Ph.D.

Alexander Lisboa-Wright

Astrophysics Research Institute, Liverpool John Moores University
September 2018

Abstract

Chapter 1

Units and terminology

Unless stated otherwise, all quantities will be described in CGS units (masses in grams, lengths in centimetres, times in seconds, energies in ergs).

M : mass
$M_\odot = 1.989 \times 10^{33}$ g : solar mass
L : luminosity
$L_\odot = 3.842 \times 10^{33}$ erg s^{-1} : solar luminosity
g : gravity
R : radius
$G = 6.6723 \times 10^{-8}$ cm^3 g^{-1} s^{-2} : gravitational constant
$\sigma_{\rm SB} = 5.678 \times 10^{-5}$ erg cm^{-2} K^{-4} s^{-1} : Stefan-Boltzmann constant

Chapter 2

Introduction

2.1 Motivation

As the light emitted from a star travels towards a distant observer, its intensity, or flux, F decreases with distance d via an inverse-square law:

$$F = \frac{L}{4\pi d^2} \tag{2.1}$$

where L is the star's luminosity, which is an intrinsic property of the star (i.e., independent of the observer). However, the interstellar medium is composed of many different structures, such as diffuse gas clouds, that can absorb or scatter light passing through, depending on the wavelength of the incoming photons, the density of the medium and the quantum levels in the atoms occupied by their electrons.

2.2 Observational constraints

No telescope can view the sky at all spectral wavelengths - it would be wholly impractical due to the sheer number of sources across the spectrum, as well as the fact that telescope resolution depends on the wavelength of the incoming light. Therefore, modern telescopes are equipped with a system of filters or bands, which allow only light within a narrow range of wavelengths. In a filter system, the individual filters are designed to operate best at different wavelengths. The system will be therefore have the following properties:

- the filters cover a much wider range of spectral wavelengths when combined than a single filter would alone; this is used to observe sources at different wavelengths to determine its spectral colour ** (see Section ***).
-

Filters - Johnson, ACS, WFC/UVIS, Gaia In this project, three broad-band filter systems were employed. These are the Advanced Camera for Surveys (ACS) and the

System	Filter	Peak wavelength / Å	FWHM / Å
ACS	F435W	4760	729
	F475W	5000	986
	F555W	5060	841
	F606W	6690	1566
	F625W	6480	978
	F775W	7320	1017
	F814W	7460	1657
WFC3	F218W	2175	300
	F225W	2250	500
	F275W	2750	500
	F300X		2775
	F336W	3375	550
	F390W	3900	1000
	F438W	4320	695
	F475W	4750	1520
	F555W	5410	1605
	F606W	5956	2340
	F625W	6250	1550
	F775W	7760	1470
	F814W	8353	2555
Gaia	G		
	G_{bp}		
	G_{rp}		

Table 2.1: Basic properties of the filters employed in this project

Ultraviolet Imaging Spectrograph channel of the Wide-Field Camera 3 (WFC3/UVIS), both mounted on the Hubble Space Telescope (HST), and the single filter set mounted on the Gaia space observatory.

ACS was installed on HST in 2002 and repaired in 2009, when WFC3 was also installed.

Filters thus*** present a challenge when trying to determine stellar spectra accurately. This task is further complicated by the fact that, even in the wavelength range where a filter does detect incoming flux, the fraction of light it detects, known as the transmittance, is not uniform across the range. The transmittance as a function of wavelength range is known as a transmission curve or filter response function. Examples of response functions for some**** of the filters employed in this project are shown in Figure 2.1. By comparing these with the filters' information in Table 2.1, it can be seen that the exact shape of the response function could have a significant impact on the observed spectrum if not taken into account. The values in the column labelled 'FWHM' represents the full width at half-maximum. In this case, it is de-

fined as the difference between the lowest and highest wavelength values at which the transmittance value is half of its maximum value for the filter, typically assuming the response function can be approximated as a Gaussian distribution. The FWHM acts as a proxy*** for the wavelength range within which the filter can reliably be used for observations.

The wavelengths of light visible to an average human eye are in the range 3800-7400 Å. Hence, the filters used here cover wavelengths from the soft-ultraviolet (soft-UV) to the near-infrared (NIR), including all visible wavelengths.

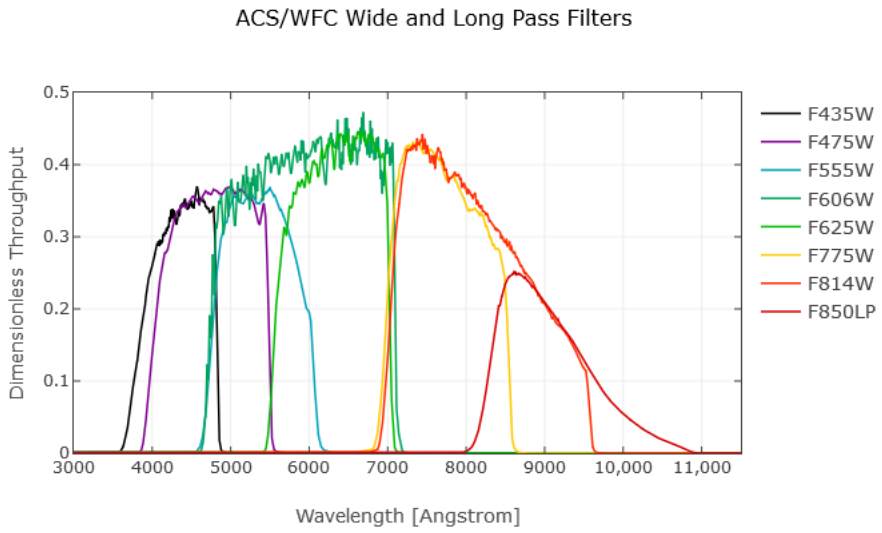

Figure 2.1: Filter response functions for wide-field ACS filters

2.3 Basics of stellar evolution

2.4 Previous studies

***Cardelli et al. (1989) produced empirical equations to accurately describe the ratio of extinction coefficients in a chosen filter X (A_X) and the Johnson-V filter (A_V), respectively. From this point onward, this ratio will be referred to as A_X/A_V.

***Girardi et al. (2008)

***Casagrande & Vandenberg (2014, 2018a, 2018b)

Chapter 3

Theory

3.1 Extinction definition

Extinction is defined using the standard astronomical system of flux magnitudes. In general, the difference between two flux measurements, F_1 and F_2, in magnitudes, is expressed as:

$$m_1 - m_2 = -2.5 \log \left(\frac{F_1}{F_2} \right) \tag{3.1}$$

where m_1 and m_2 are the magnitudes for F_1 and F_2, respectively. However, the flux of a source varies naturally with the distance to the observer (see Equation 2.1). To account for this, the distances to the nearest stars was determined independently of their flux, by their parallax from Earth. This gives each astronomical object two characteristic flux measurements. These are the apparent magnitude, m, and the absolute magnitude, M. The apparent magnitude is the flux magnitude of a source, as observed by the telescope. The absolute magnitude is the projected flux magnitude of the same source if it were to be placed at a distance of 10 parsecs (pc) from the telescope, thus accounting for the distances The relation between these quantities if there is zero extinction can be found by combining Equations 2.1 and 3.1:

$$m - M = -2.5 \log \left((\frac{10\text{pc}}{d})^2 \right) = 5log((d/\text{pc}) - 5 \tag{3.2}$$

The quantity $(m-M)$ is known as the distance modulus. It is particularly useful for observing stellar populations, as stars within a single-age population are easily classified using their position on the theoretical Hertzsprung-Russell (HR) diagram or ***some of its observational equivalents, known as colour-magnitude diagrams (CMDs). In the HR diagram, stars of a given age and metallicity are plotted in the luminosity-effective temperature ($L - T_{\text{eff}}$) plane. An example of a HR diagram is shown in Figure ****. It can be seen that all stars lie on a single, complicated line, known as an isochrone. Isochrones for different population ages and metallicities are calculated using theoretical stellar models for the largest possible spread of initial stellar masses. An isochrone in the HR diagram has a number of distinct features:

- Most stars, including the coolest and least-luminous ones, follow a tight pattern of luminoaity increasing with temperature. This is known as the main sequence (MS)
- This pattern stops as the luminosity continues to increase slowly but with decreasing temperature. The end of the MS is called the main-sequence turn-off (MSTO), which is followed by the sub-giant branch (SGB).
- After the SGB, the gradient becomes much steeper, with temperate decreasing and luminosity rapidly increasing. This is the red-giant branch (RGB).
- At the tip of the RGB, stars start becoming fainter and their temperatures increase. Eventually, their is a sequence of stars with near-constant luminosity but a range of effective temperatures. This is the horizontal branch (HB).
- After the horizontal branch, there is again a rapid increase in luminosity accompanied by a slow decrease in temperature. This is the asymptotic giant branch (AGB).

It should be noted that the distance modulus in Equation 3.2 does not include extinction. To link the apparent magnitude to extinction, it is necessary to separate the distance modulus from the observed apparent magnitude, $m_{\rm obs}$. This can be done by defining the intrinsic apparent magnitude, m_0, such that:

$$m_0 - M = 5\log((d/\mathrm{pc}) - 5 \tag{3.3}$$

i.e., the distance modulus is solely dependent on the distance to the sources. Therefore, the extinction A can be defined as:

$$A = m_{\rm obs} - m_0 \tag{3.4}$$

This fits with the definition of interstellar extinction given earlier, i.e. as the flux lost solely due to scattering and absorption in the interstellar medium.

3.2 Bolometric corrections

All the equations in Section ****, including those for extinction, are not useful when applied to telescopes, as any filter will only detect a small fraction of the stellar flux across all wavelengths (known as the bolometric stellar flux) that reaches the telescope. The missing information resulting from this observational constraint renders it difficult to determine the interstellar extinction. These constraints much be mitigated before an accurate value of the extinction coefficient can be determined. Bolometric corrections are employed for this purpose.

The use of bolometric corrections requires the detailed knowledge of stellar spectra least susceptible to significant extinction, i.e., nearby stars with high apparent fluxes.

Only with complete knowledge of the spectrum from a reference star can the true spectrum of a distant star with unknown extinction be calculated. The spectra of these stars can be computed by using a grid of predicted fluxes from a stellar atmosphere model, the grid being composed of the stellar parameters known to change emission in stellar atmospheres. These are effective temperature, surface gravity and metallicity. For all filter systems studied in this project, the nearby star Vega was used as the reference object.

The effective temperature ($T_{\rm eff}$) of a star is defined as the temperature of a black body which produces the closest matching bolometric spectrum to that of the star. This approximation is valid because all stars have been observed to have spectra that closely resemble those of black bodies, with the notable exception of atmospheric absorption lines.

$$L = 4\pi R^2 \sigma_{SB} T_{\rm eff}^4 \tag{3.5}$$

Effective temperature has an effect on interstellar extinction due to its strong effect on the stellar luminosity and, hence, the flux. For a higher flux, more photons are likely to interact with the ISM, hence a higher extinction coefficient.

The metallicity of a star is defined as the fractional abundance of heavy elements, often approximated by iron alone, relative to the star's hydrogen abundance, compared to that of the Sun. The abundances are determined by the strength of the elements' characteristic atomic absorption lines in the stellar spectra.

$$[{\rm Fe/H}] = \log(N_{\rm Fe}/N_{\rm H}) - \log(N_{\rm Fe,\odot}/N_{\rm H,\odot}) \tag{3.6}$$

Since the output is logarithmic, a value of $[{\rm Fe/H}] = 0$ indicates solar metallicity. An increase in metallicity would cause the corresponding absorption lines to be stronger, thus reducing the observable flux.

The definition of the stellar surface gravity g is simply the value of the standard Newtonian gravtitional acceleration, applied to the stellar surface (the mass is the total stellar mass, M_*, and the distance is the stellar radius, R_*):

$$g = \frac{GM_*}{R_*^2} \tag{3.7}$$

A higher surface gravity represents a surface with a higher atomic number density. This environment produces a shorter mean free path for photons overall, meaning a smaller collision timescale. If the timescale is sufficiently small, the limit provided by Heisenberg's Uncertainty Principle causes an increase in the uncertainty of the energy absorbed by the atomic electron during the interaction with the photon:

$$\Delta E \Delta t \geq \hbar/2 \tag{3.8}$$

This effect, known as "pressure broadening", causes a symmetrical distribution of absorption energies (and wavelengths) about the normal emission energy for that particular atomic state. This means fewer photons pass through the surface, thereby reducing the surface flux.

After accounting for a general extinction effect on an object's emission, its apparent magnitude in a given filter X (i.e. wavelength range, which we define as increasing from λ_1 to λ_2) is given by:

$$m_X = -2.5 \log_{10} \left(\frac{\int_{\lambda_1}^{\lambda_2} f_\lambda \left(10^{-0.4 A_{X,\lambda}}\right) S_\lambda d\lambda}{\int_{\lambda_1}^{\lambda_2} f_\lambda^0 S_\lambda d\lambda} \right) + m_X^0 \tag{3.9}$$

where f_λ represents the monochromatic flux at a given wavelength λ at the observer distance, $A_{X,\lambda}$ is the extinction value as a function of wavelength, S_λ represents the filter response function and f_λ^0 and m_X^0 represent the monochromatic flux and apparent magnitude, respectively, of a known reference object in X.

To derive the equation linking a bolometric correction with the extinction parameter, we start with the definition of a bolometric correction in a filter X, which is denoted by BC_X:

$$BC_X \equiv M_{\text{bol}} - M_X \tag{3.10}$$

where M_X is the absolute magnitude of the object in X and M_{bol} is its (predicted) absolute bolometric magnitude, defined relative to the Sun using:

$$M_{\text{bol}} = M_{\text{bol},\odot} - 2.5 \log_{10} \left(\frac{4\pi R^2 F_{\text{bol}}}{L_\odot} \right) \tag{3.11}$$

where F_{bol} is the bolometric stellar flux at its surface, R is the stellar radius, $M_{\text{bol},\odot}$ is the solar absolute bolometric magnitude, which is assumed in this work to have a value of 4.75 and $L_\odot$ is the solar luminosity, for which a value of 3.844×10^{33} erg s^{-1} is used. Bolometric corrections can be expressed as a function of extinction using the universal definition of M_X in terms of m_X and the distance d to the source:

$$M_X = m_X - 2.5 \log_{10} \left(\left(\frac{d}{10\text{pc}} \right)^2 \right), \tag{3.12}$$

together with the equation $f_\lambda d^2 = F_\lambda R^2$, where F_λ is the monochromatic flux at λ at the stellar surface. This gives the final function for a bolometric correction for filter X:

$$\begin{aligned} BC_X = M_{\text{bol},\odot} - m_X^0 - 2.5 \log_{10} \left(\frac{4\pi R^2 F_{\text{bol}}}{L_\odot} \right) \\ + 2.5 \log_{10} \left(\frac{\int_{\lambda_1}^{\lambda_2} F_\lambda \left(10^{-0.4 A_{X,\lambda}}\right) S_\lambda d\lambda}{\int_{\lambda_1}^{\lambda_2} f_\lambda^0 S_\lambda d\lambda} \right) \end{aligned} \tag{3.13}$$

For a filter X, the extinction parameter $A_X = A_{X,\lambda}$ must be calibrated relative to a known value. In this work we will input a value of the extinction in the well-studied Johnson-V filter, A_V. To extract A_X, we use the simple relation:

$$A_X = \left(\frac{A_X}{A_V}\right) A_V \tag{3.14}$$

together with the chosen value of A_V (for this project the values were $A_V = 0$, 1 - note that $BC_X(A_V = 0)$ effectively assumes no extinction), before taking the difference between the two $BC_X(A_V)$, giving the following equation:

$$\begin{aligned} BC_X(0) - BC_X(A_V) &= 2.5 \log_{10} \left(\frac{\int_{\lambda_1}^{\lambda_2} F_\lambda S_\lambda d\lambda}{\int_{\lambda_1}^{\lambda_2} F_\lambda \left(10^{-0.4\left(A_{X,\lambda}/A_V\right)A_V}\right) S_\lambda d\lambda} \right) \\ &\approx \left(A_X/A_V\right) A_V \end{aligned} \tag{3.15}$$

****average over the wavelength interval $[\lambda_1, \lambda_2]$ which is a valid assumption (**?**), even for the wide-field Hubble filters being studied in this work.

Chapter 4

Methodology

4.1 Software used

Python 2.7 FORTRAN 77 code ATLAS9 BaSTI

4.2 Finding & fitting functions

Guesswork!

4.3 Isochrone data fitting

****BaSTI models - transforming grid variables The output from the BaSTI database for each model stellar object gives the model's initial mass and current mass (i.e. after a time equal to the ischrone age), together with the logarithms of the stellar luminosity in solar units ($\log_{10} L/L_{\odot}$) and of the effective temperature in K ($\log_{10} T_{\rm eff}$). To derive the surface gravity g, we must combine Equations 3.5 (to derive the stellar radius) 3.7. Equation 4.1 shows the resultant definition of g in cgs units:

$$g = \frac{4\pi G M_* \sigma_{\rm SB} T_{\rm eff}^4}{L_*} \tag{4.1}$$

DR2 Babusiaux data, errors

Isochrone (Age/Myr , [Fe/H])	T_{eff} minimum	T_{eff} maximum	$\log(g)$ minimum	$\log(g)$ maximum
500,0.002	2870	9640	0.886	5.137
1000,0.002	2824	8035	1.608	5.184
5000,-1.049	3118	7112	0.456	5.318
10000,-1.049	3086	6412	0.286	5.332

Table 4.1: Ranges of effective temperature and surface gravities in selected BaSTI isochrones

Chapter 5

Results and discussion

5.1 Extinction coefficient models

It should be noted that the

5.2 Effect on isochrones

Given the large number of filters studied in Section 5.1, four commonly-used CMD axes were selected to test for any effects of a function-derived A_X. Two of these are specific to the WFC3 system, with one CMD each for ACS and Gaia.

5.2.1 ACS

The CMD chosen for the ACS was the F435W-(F435W-F814W) axis combination. This CMD is useful as it pairs the bluest and reddest wide-field filters for the ACS, which produces larger spectral colours.****

5.2.2 WFC3

The CMD chosen for the ACS was the F435W-(F435W-F814W) axis combination. This CMD is useful as it pairs the bluest and reddest wide-field filters for the ACS, which produces larger spectral colours.****

5.2.3 Gaia

Given that Gaia has only three photometric filters in total and given that the G_{bp} and G_{rp} was the F435W-(F435W-F814W) axis combination. This CMD is useful as it pairs the bluest and reddest wide-field filters for the ACS, which produces larger spectral colours.****

System	Filter	A_1 function	A_1 coefficients		
			a	b	c
ACS	F435W	pow	-(3.381±0.733)×10^4	-1.394±0.026	1.040±0.001
	F475W	pow	-457.6±64.9	-0.9000±0.0172	1.247±0.002
	F555W	pow	-(4.383±0.871)×10^3	-1.361±0.023	0.6771±0.0002
	F606W	pow	-(4.383±0.871)×10^3	-1.361±0.023	0.6771±0.0002
	F625W	pow	-(3.381±0.733)×10^4	-1.394±0.026	1.040±0.001
	F775W	pow	-457.6±64.9	-0.9000±0.0172	1.247±0.002
	F814W	pow	-(4.383±0.871)×10^3	-1.361±0.023	0.6771±0.0002
WFC3	F218W	exp	-232.4±48.1	-(1.076±0.043)×10^{-3}	2.933±0.007
	F225W	exp	-128.5±13.8	-(1.031±0.022)×10^{-3}	2.610±0.003
	F275W	exp	0.9726±0.0581	-(3.518±0.109)×10^{-4}	2.060±0.001
	F300X	pow	-(5.335±0.936)×10^5	-1.664±0.021	2.052±0.001
	F336W	pow	-(1.516±0.723)×10^4	-1.582±0.056	1.648±0.001
	F390W	pow	-0.5991±0.1494	-0.08071±0.09090	1.738±0.309
	F438W	pow	-(1.000±0.463)×10^5	-1.783±0.054	1.352±0.001
	F475W	pow	-(1.207±0.379)×10^5	-1.707±0.037	1.220±0.001
	F555W	pow	-(4.560±1.490)×10^5	-1.881±0.038	1.080±0.001
	F606W	pow	-(3.137±0.911)×10^5	-1.829±0.034	0.9648±0.0003
	F625W	pow	-(5.476±3.709)×10^5	-2.030±0.079	0.8787±0.0002
	F775W	pow	-(6.328±4.571)×10^3	-1.576±0.085	0.6567±0.0001
	F814W	pow	-(3.727±1.381)×10^3	-1.431±0.044	0.6158±0.0002
Gaia	G	pow	-(3.381±0.733)×10^4	-1.394±0.026	1.040±0.001
	G_{bp}	pow	-457.6±64.9	-0.9000±0.0172	1.247±0.002
	G_{rp}	pow	-(4.383±0.871)×10^3	-1.361±0.023	0.6771±0.0002

Table 5.1: Coefficient values produced by A_1 fitting

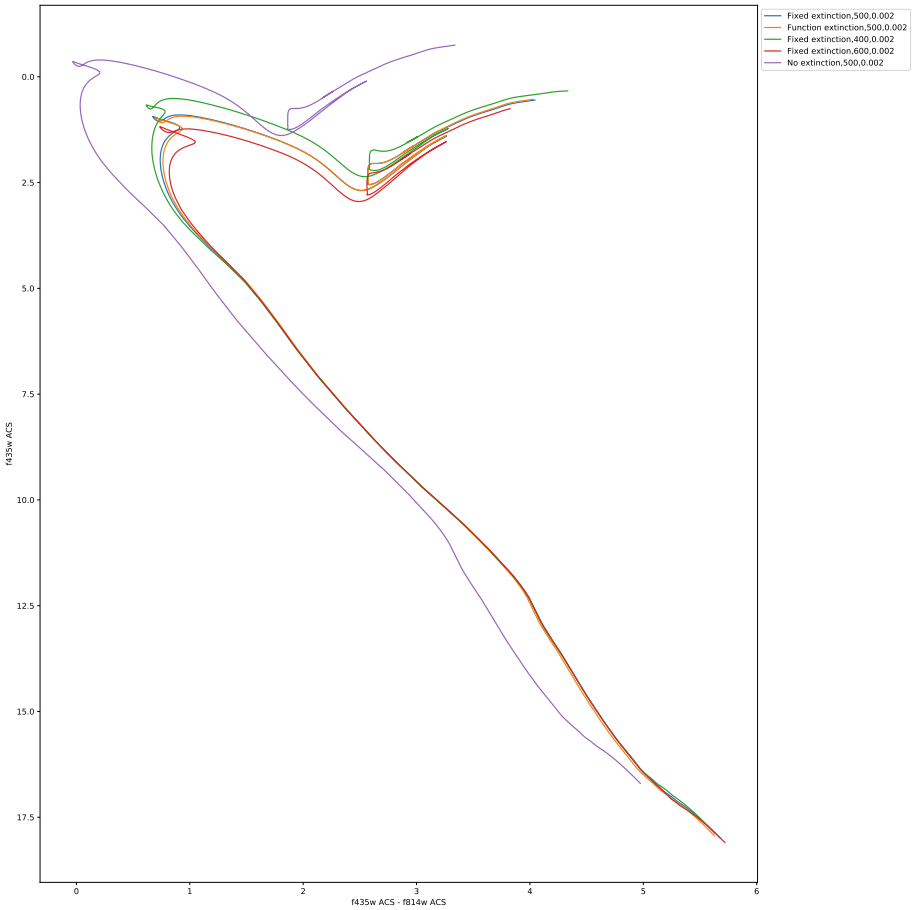

Figure 5.1: Ratios of A_X/AV values for different Z values compared with solar metallicity data at $\log(g) = 5.0$

5.3 Test case: NGC 6793

To test the effects of the difference in treatment of A_X/AV, both cases were employed to predict the isochrone ***parameters of the open cluster NGC 6793.

5.3.1 Observational background

NGC 6793 has little information available compared to many other open clusters. Two estimates for observational properties of the cluster have been published and are listed in Table 5.2.

5.3.2 Comparison of extinction methods

The Gaia DR2 dataset, containing the parallaxes and apparent magnitudes (in all three Gaia filters) for 338 objects tagged as belonging to NGC 6793, was obtained.

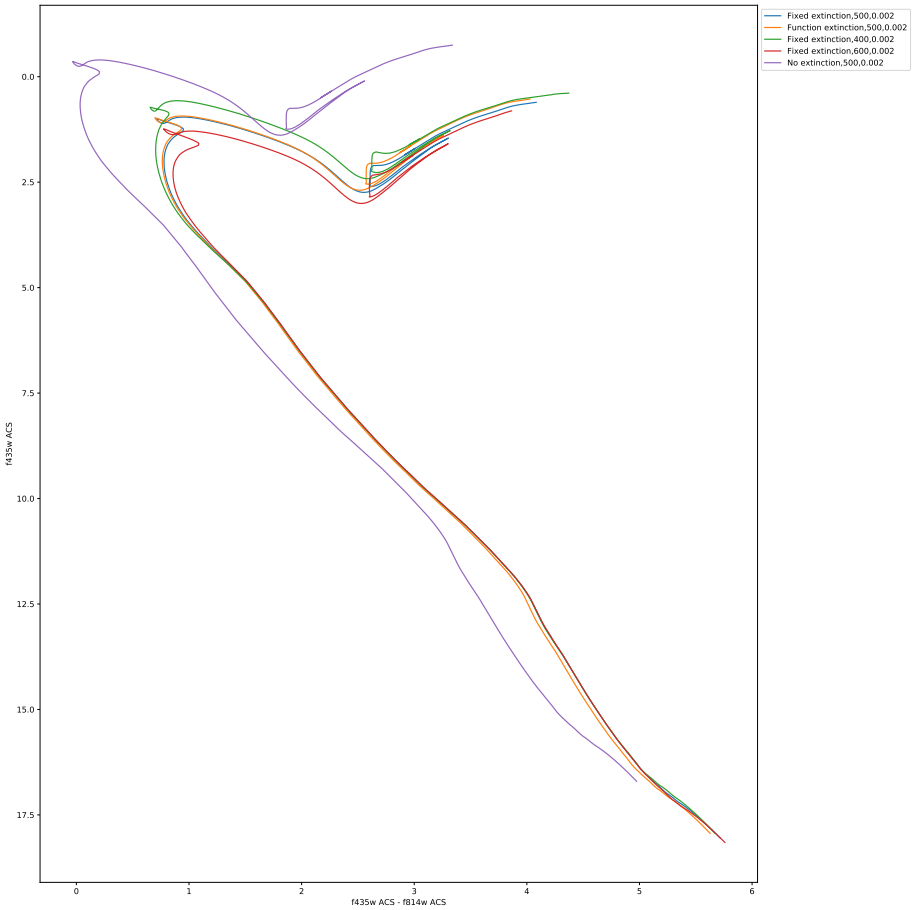

Figure 5.2: Ratios of A_X/AV values for different Z values compared with solar metallicity data at $\log(g) = 5.0$

The number of objects is greater than the 271 photometric Gaia objects found by Gaia Collaboration et al. (2018). There were significant variations in the observed parallaxes of individual stars, far beyond the maximum cluster radii expected (Schilbach et al. (2006) - general open cluster properties).

There are highly significant errors for the individual objects in the Gaia data propagation, even when assuming the only source of error is from parallax measurements (see Figure 5.9). The magnitude of the errorbars dwarf any changes in isochrones due to extinction coefficient treatments.

All, as shown in Section****, the isochrones are sensitive both to the reference extinction coefficient value A_V and to the value of A_X/A_V for the fixed case. Some individual parts of the isochrones relevant to this study are additionally sensitive to other isochrone parameters:

1. The position of the MSTO is sensitive to the treatment of A_X/A_V, as shown in Section****, and the isochrone age.

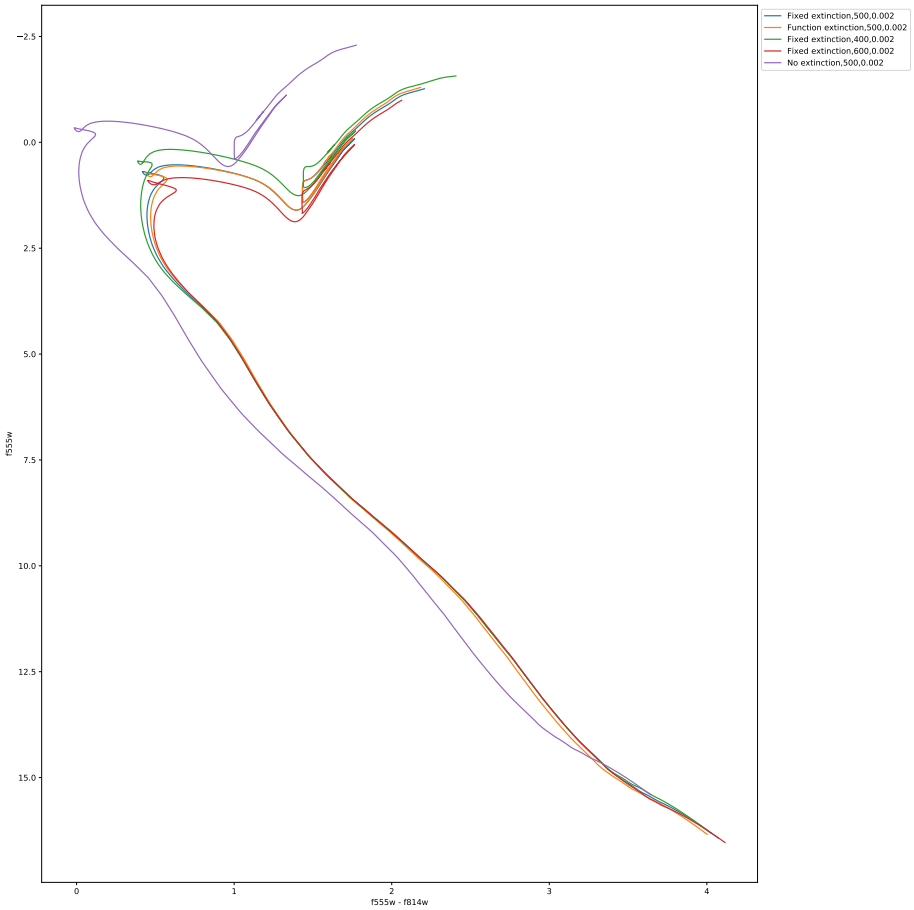

Figure 5.3: Ratios of A_X/AV values for different Z values compared with solar metallicity data at $\log(g) = 5.0$

2. The position of the lower main sequence is significantly more sensitive to metallicity than other parts of the isochrone.

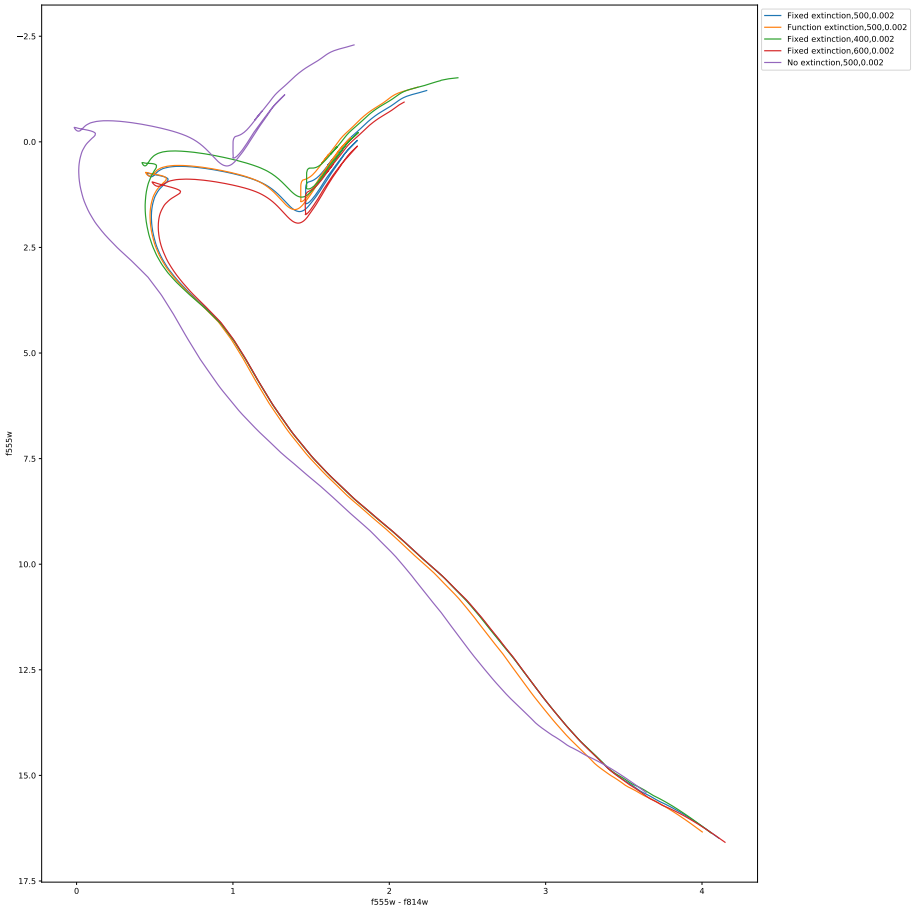

Figure 5.4: Ratios of A_X/AV values for different Z values compared with solar metallicity data at $\log(g) = 5.0$

Cluster property	K05	GC18
Distance modulus / mag	10.73	8.894
-> distance / pc	1400	601
log(age / yr)	8.64	8.78
-> Age / Myr	437	603
$E(B-V)$ / mag	0.17	0.272
$[Fe/H]$	?	?
Members	? ($>$ 3 ACSS-2.5)	465 (271 with Gaia photometry)

Table 5.2: Observational parameters for NGC 6793, according to Kharchenko et al. (2005) (WEBDA archive page) and Gaia Collaboration et al. (2018)

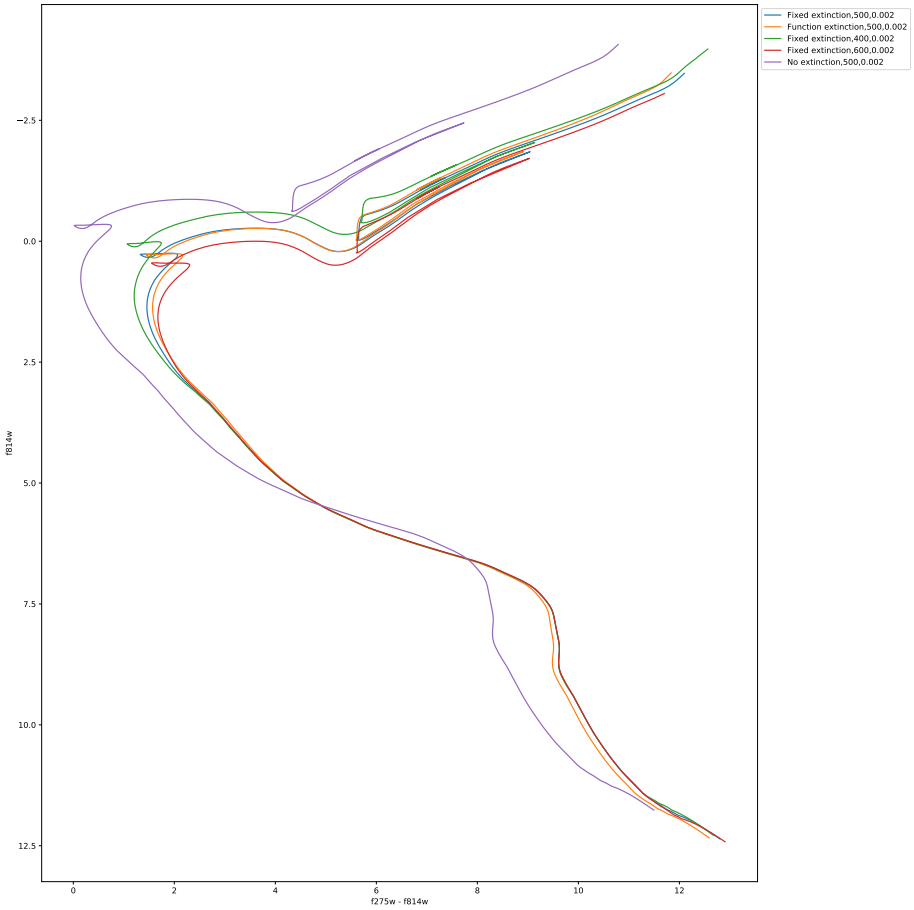

Figure 5.5: Ratios of A_X/AV values for different Z values compared with solar metallicity data at $\log(g) = 5.0$

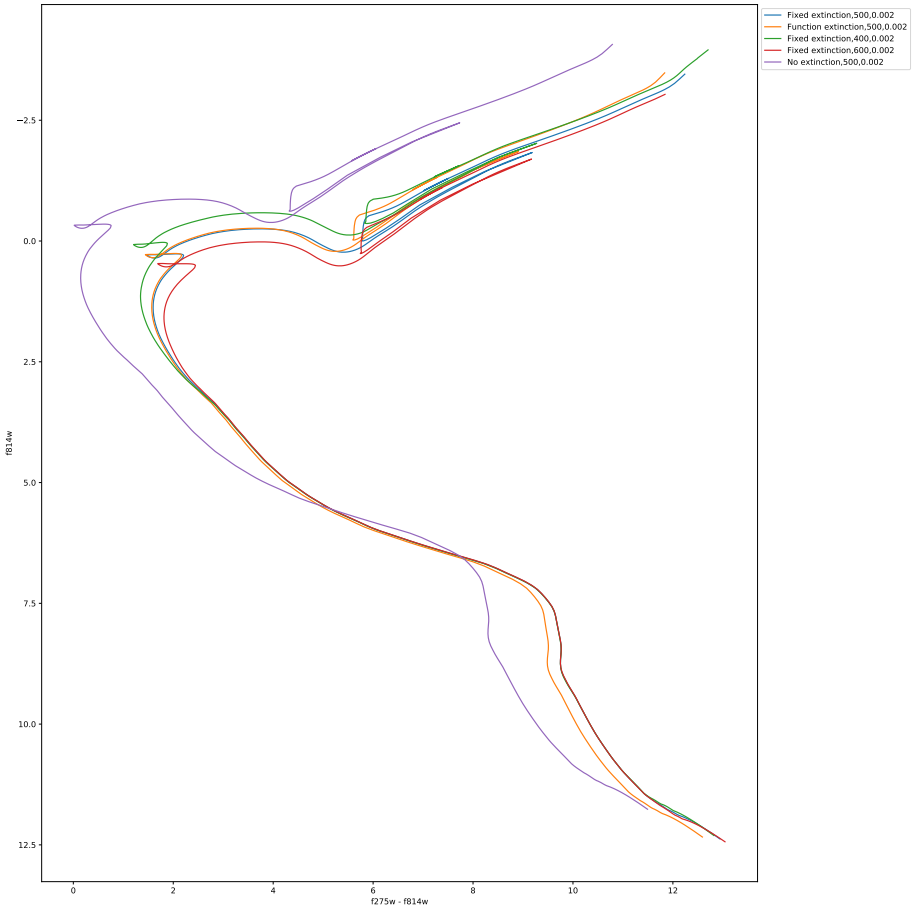

Figure 5.6: Ratios of A_X/AV values for different Z values compared with solar metallicity data at $\log(g) = 5.0$

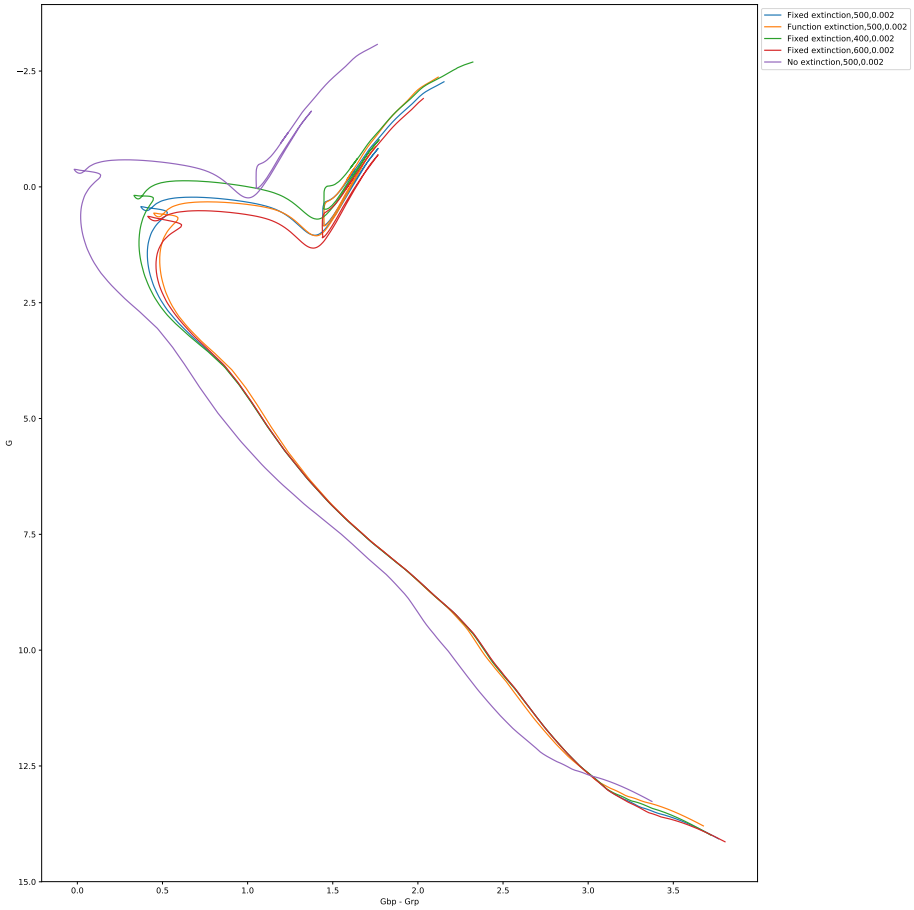

Figure 5.7: Ratios of A_X/AV values for different Z values compared with solar metallicity data at $\log(g) = 5.0$

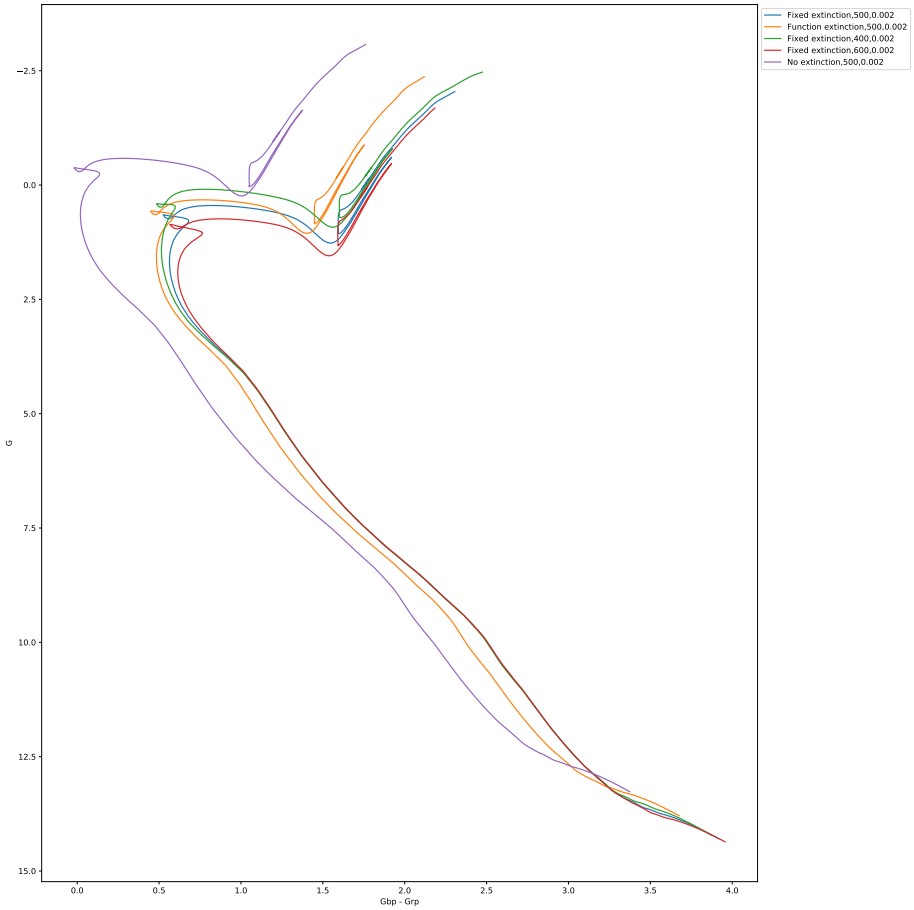

Figure 5.8: Ratios of A_X/AV values for different Z values compared with solar metallicity data at $\log(g) = 5.0$

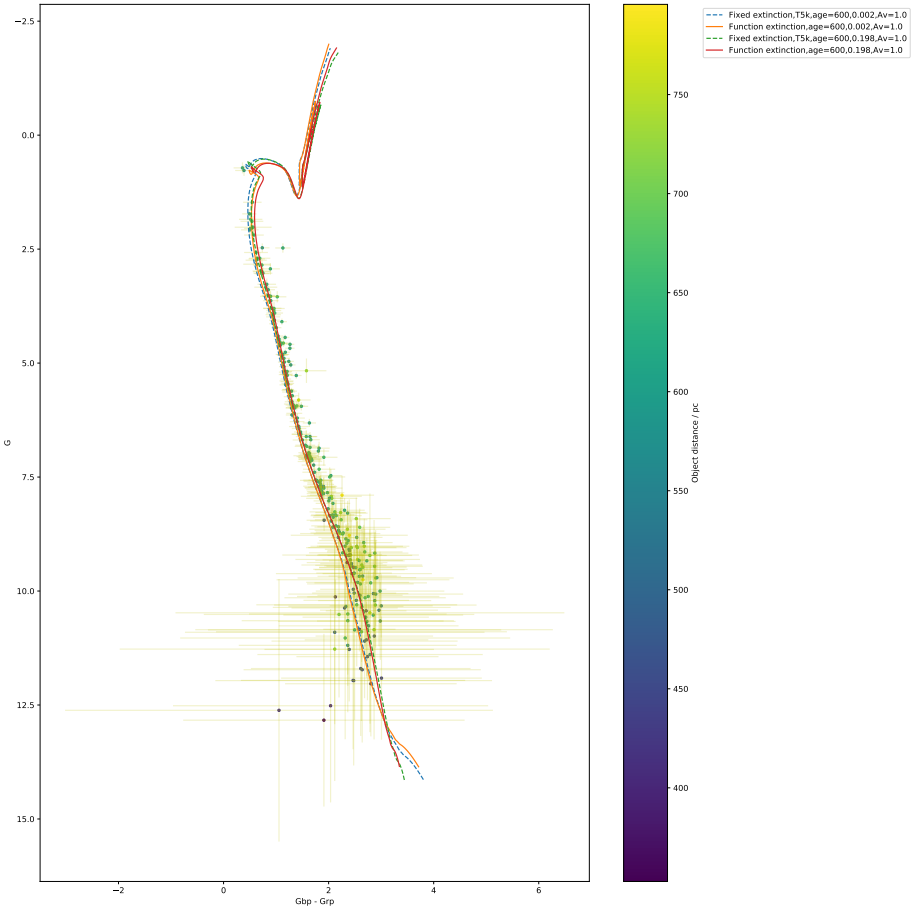

Figure 5.9: Gaia CMD of NGC 6793 with errorbars included.

Chapter 6

Conclusion

In all cases, applying a fixed extinction to all points in an isochrone causes the main-sequence turn-off to occur at a more luminous, bluer point in a given CMD than the MSTO point for an extinction coefficient described using a function fitted to empirically derived data.

6.1 Future work

Bibliography

Gaia Collaboration et al., 2018, http://dx.doi.org/10.1051/0004-6361/201832843 A&A, http://adsabs.harvard.edu/abs/2018A

Girardi L., et al., 2008, PASP, 120, 583

Kharchenko N. V., Piskunov A. E., Röser S., Schilbach E., Scholz R.-D., 2005, http://dx.doi.org/10.1051/0004-6361:20042523 A&A, http://adsabs.harvard.edu/abs/2005A

Schilbach E., Kharchenko N. V., Piskunov A. E., Röser S., Scholz R.-D., 2006, http://dx.doi.org/10.1051/0004-6361:20054663 A&A, http://adsabs.harvard.edu/abs/2006A